

 Open access • Journal Article • DOI:10.1021/ACSNANO.7B04868

Dielectric Meta-Holograms Enabled with Dual Magnetic Resonances in Visible Light.

— [Source link](#) 

Zile Li, Inki Kim, Lei Zhang, Muhammad Qasim Mehmood ...+10 more authors





Institutions: Wuhan University, Pohang University of Science and Technology, Xi'an Jiaotong University, University of the Punjab ...+5 more institutions

Published on: 14 Sep 2017 - ACS Nano (American Chemical Society)

Topics: Magnetic dipole, Dielectric and Holography

Related papers:

- [Metasurface holograms reaching 80% efficiency](#)
- [Light Propagation with Phase Discontinuities: Generalized Laws of Reflection and Refraction](#)
- [Metalenses at visible wavelengths: Diffraction-limited focusing and subwavelength resolution imaging.](#)
- [Dielectric metasurfaces for complete control of phase and polarization with subwavelength spatial resolution and high transmission](#)
- [Full-space Cloud of Random Points with a Scrambling Metasurface.](#)

Share this paper:    

View more about this paper here: <https://typeset.io/papers/dielectric-meta-holograms-enabled-with-dual-magnetic-11sa8une27>

Dielectric Meta-Holograms Enabled with Dual Magnetic Resonances in Visible Light

Zile Li, Inki Kim, Lei Zhang, Muhammad Q Mehmood, Muhammad S Anwar, Murtaza Saleem, Dasol Lee, Ki Tae Nam, Shuang Zhang, Boris S. Luk'yanchuk, Yu Wang, Guoxing Zheng, Junsuk Rho, and Cheng-Wei Qiu

ACS Nano, **Just Accepted Manuscript** • DOI: 10.1021/acsnano.7b04868 • Publication Date (Web): 12 Sep 2017

Downloaded from <http://pubs.acs.org> on September 13, 2017

Just Accepted

“Just Accepted” manuscripts have been peer-reviewed and accepted for publication. They are posted online prior to technical editing, formatting for publication and author proofing. The American Chemical Society provides “Just Accepted” as a free service to the research community to expedite the dissemination of scientific material as soon as possible after acceptance. “Just Accepted” manuscripts appear in full in PDF format accompanied by an HTML abstract. “Just Accepted” manuscripts have been fully peer reviewed, but should not be considered the official version of record. They are accessible to all readers and citable by the Digital Object Identifier (DOI®). “Just Accepted” is an optional service offered to authors. Therefore, the “Just Accepted” Web site may not include all articles that will be published in the journal. After a manuscript is technically edited and formatted, it will be removed from the “Just Accepted” Web site and published as an ASAP article. Note that technical editing may introduce minor changes to the manuscript text and/or graphics which could affect content, and all legal disclaimers and ethical guidelines that apply to the journal pertain. ACS cannot be held responsible for errors or consequences arising from the use of information contained in these “Just Accepted” manuscripts.

Dielectric Meta-Holograms Enabled with Dual Magnetic Resonances in Visible Light

Zile Li,^{‡,♯} Inki Kim,^{§,♯} Lei Zhang,^{‡,♯} Muhammad Q. Mehmood,^{#,♯} Muhammad S. Anwar,[&] Murtaza Saleem,[&] Dasol Lee,[§] Ki Tae Nam,[∇] Shuang Zhang,[⊥] Boris Luk'yanchuk,[£] Yu Wang,[‡] Guoxing Zheng,^{‡,§,*} Junsuk Rho,^{§,•,*} and Cheng-Wei Qiu^{⊥,*,*}

[‡]School of Electronic Information, Wuhan University, Wuhan 430072, China

[§]Department of Mechanical Engineering, Pohang University of Science and Technology (POSTECH), Pohang 37673, Republic of Korea

[‡]Key Laboratory for Physical Electronics and Devices of the Ministry of Education & Shaanxi Key Lab of Information Photonic Technique, Xi'an Jiaotong University, Xi'an 710049, China

[#]Department of Electrical Engineering, Information Technology University of the Punjab, Ferozpur Road, 54000 Lahore, Pakistan

[&]Department of Physics, Syed Babar Ali School of Science and Engineering (SBASSE), Lahore University of Management Sciences (LUMS), Opposite Sector U, D.H.A. Lahore 54792, Pakistan

[∇]Department of Materials Science and Engineering, Seoul National University, Seoul 08826, Republic of Korea

[⊥]School of Physics & Astronomy, University of Birmingham, Birmingham B15 2TT, UK

[‡]Data Storage Institute, A*STAR (Agency for Science, Technology and Research), 2 Fusionopolis Way, #08-01, Innovis 138634, Singapore

[§]State Key Laboratory of Optical Communication Technologies and Networks, Wuhan Research Institute of Posts & Telecommunications, Wuhan 430074, China

[•]Department of Chemical Engineering, Pohang University of Science and Technology (POSTECH), Pohang 37673, Republic of Korea

[/]Department of Electrical and Computer Engineering, National University of Singapore, 4 Engineering Drive 3, Singapore, 117583, Singapore

⁼SZU-NUS Collaborative Innovation Center for Optoelectronic Science and Technology, Shenzhen University, Shenzhen 518060, China

ABSTRACT: Efficient transmission-type meta-holograms have been demonstrated using high-index dielectric nanostructures based on Huygens' principle. It is crucial that the geometry size of building blocks needs to be judiciously optimized individually for spectral overlap of electric and magnetic dipoles. In contrast, reflection-type meta-holograms using the metal/insulator/metal scheme and geometric phase can be readily achieved with high efficiency and small thickness. Here, we demonstrate a general platform for design of dual magnetic resonance-based meta-holograms based on the geometric phase using silicon nanostructures that are quarter wavelength thick for visible light. Significantly, the projected holographic image can be unambiguously observed without a receiving screen even under the illumination of natural light. With the facilitation of the well-developed semiconductor industry, our ultra-thin magnetic resonance-based meta-holograms may have promising applications in anti-counterfeiting and information security.

1
2
3 KEYWORDS: *metasurfaces, dielectric nanostructures, magnetic resonance, image hologram*
4
5
6
7
8

9 Metasurfaces have led to many unconventional optical properties as well as novel physical
10 phenomena and applications.¹⁻³² In particular, geometric metasurfaces (GEMSs) based on the
11 Pancharatnam-Berry phase have attracted extensive attention due to their simple and robust
12 phase control scheme.¹⁶⁻³² The beauty of this approach lies in the linear dependence of phase
13 delay φ on the orientation angle α of each nanostructure, *i.e.*, $\varphi = \pm 2\alpha$, with the sign determined by
14 the polarity of incident light.^{22, 31} At the same time, the scattering amplitude remains unchanged
15 since the geometry remains consistent. Therefore, GEMSs offer new perspectives in designing
16 complex phase-only optical elements, such as holograms,²⁵⁻³⁴ which have been investigated in
17 the visible and infrared ranges using noble metal nanostructures.^{33, 34} For example, a reflection-
18 type hologram based on the hybrid of geometric phase and gap plasmon has been realized with
19 high efficiency using metal-insulator-metal (MIM) structures.^{31, 32} However, the intrinsic ohmic
20 loss of metals is still severe at short visible frequency, which may deteriorate the total efficiency.
21
22 Therefore, low-loss or even lossless dielectrics represent a promising material route towards high
23 performance GEMSs.²⁰⁻²⁶ Nevertheless, dielectric GEMSs usually suffer from requirements of
24 larger structural heights, in sharp contrast to metal GEMSs. For instance, the height of current
25 dielectric structures is $\sim\lambda$ for TiO₂^{23, 24} and $\sim\lambda/1.7$ for silicon,²² while that of metal structures can
26 be as small as $\sim\lambda/27$.³¹ Consequently, high aspect ratio (AR), defined as the ratio of height to
27 width, for instance, 6.3~15 for TiO₂^{23, 24} in the visible range and 4.8 for silicon²² in fiber
28 telecommunication windows, is unavoidable for building blocks of GEMSs. The challenge in
29 high AR seriously increases the fabrication burden and renders the device less compact.
30
31
32
33
34
35
36
37
38
39
40
41
42
43
44
45
46
47
48
49
50
51
52
53
54
55
56
57
58
59
60

1
2
3 Although atomic layer deposition (ALD) enables fabrication of high AR dielectric
4 nanostructures,²⁴ it is still challenging to realize large-scale and cost-efficient samples.
5
6

7
8
9 Even though the generation of geometric phase is independent of the specific size, introduction
10 of a resonant mode is also beneficial for optimized efficiency at a given wavelength. Lately,
11 optical magnetic modes have been observed in high index insulators in the visible frequency
12 range.³⁵⁻⁴¹ In particular, by matching the electric dipole mode and magnetic dipole in frequency
13 domain, Huygens' metasurfaces were demonstrated to manipulate transmitted light with high
14 efficiency.^{42, 43} According to Mie theory, at given wavelength, the structure supporting a
15 magnetic dipole mode has an even smaller size in comparison with the counterpart supporting an
16 electric dipole mode. As a result, magnetic resonance is useful for shrinking the AR of structures
17 for compact GEMSs design. Moreover, the scattering cross section of magnetic dipole mode is
18 also superior to the electric counterpart, a higher manipulation efficiency is thus expected.
19
20
21
22
23
24
25
26
27
28
29
30
31
32

33
34 In this work, we demonstrate a silicon (Si) GEMS by combining geometric phase and magnetic
35 resonance. The height of building blocks is dramatically reduced down to a quarter of the
36 operation wavelength, while all advantages of conventional GEMSs are preserved. Three
37 examples are presented to verify our proposal, including a Fourier hologram and two image
38 holograms. For image holograms, clear holographic images can be observed under arbitrary
39 illumination condition such as natural light, which greatly facilitate practical applications under
40 loose requirements of illumination. In addition, superior image hologram performance is also
41 demonstrated by Si GEMSs fabricated on silicon on insulator (SOI), which indicates a good
42 compatibility with the mature semiconductor industry.
43
44
45
46
47
48
49
50
51
52
53
54
55
56
57
58
59
60

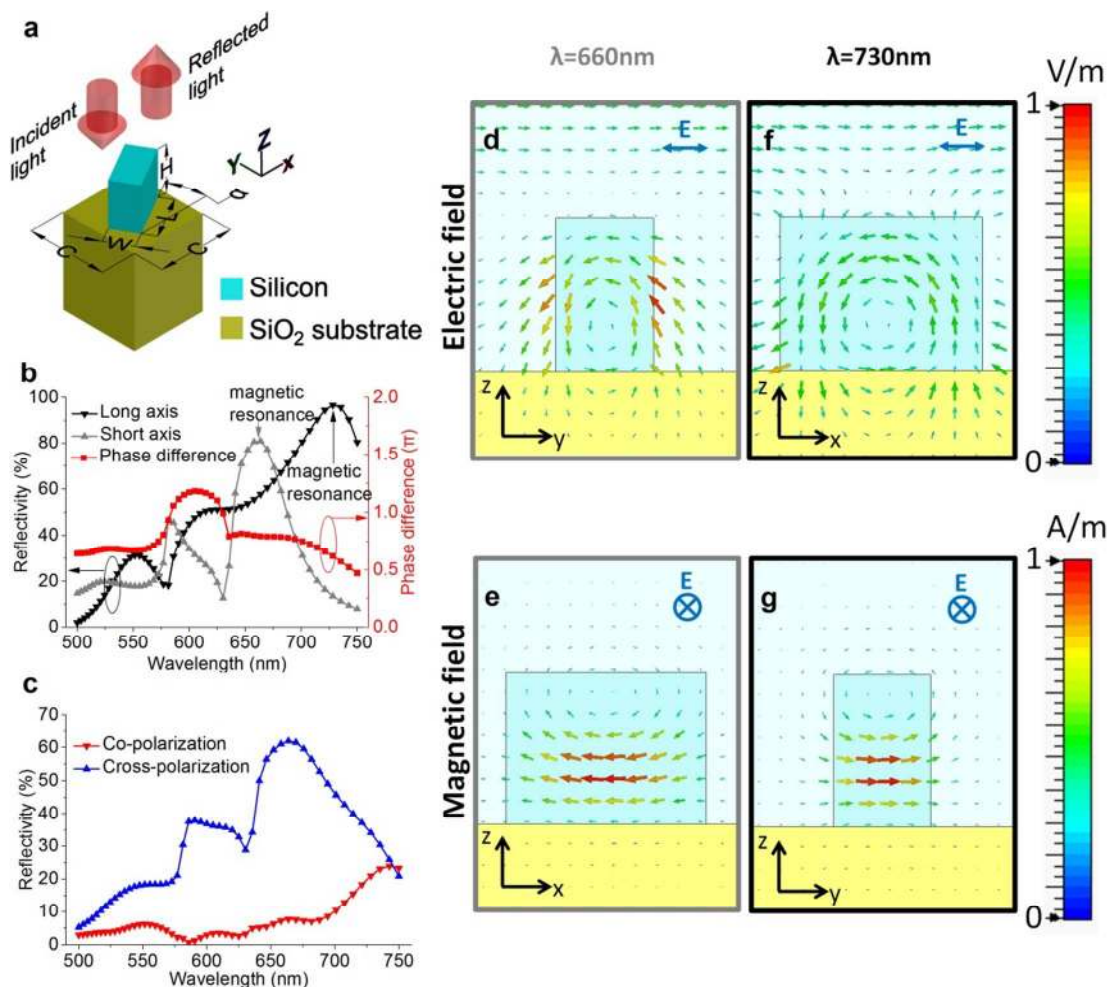


Figure 1. Illustration and simulated results of the unit cell. **a**, Schematic of one unit cell of the resonant GEMS. **b**, Simulated reflectivity and phase difference of the nanobrick when the normal incident beam is polarized along the long axis and short axis of the nanobrick, respectively. **c**, Simulated reflectivity of the cross-polarized and co-polarized parts under normal light incidence with circular polarization. **d**, **e**, The vortex-like normalized electric field and enhanced magnetic field distribution at the cross-section of a nanobrick unit-cell when the incident electric field is polarized along y-axis at wavelength of 660 nm. **f**, **g**, The vortex-like normalized electric field and enhanced magnetic field distribution at the cross-section of a nanobrick unit-cell when the incident electric field is polarized along x-axis at wavelength of 730 nm. Polarization of incident light is indicated insets in **d-g**.

Figure 1a shows the schematic of the adopted unit cell of our GEMS. Geometric phase is generated under illumination with circular polarization, and the phase delay can only be imparted

1
2
3 to the reflected light with opposite polarity. Therefore, an efficient polarization conversion
4 results in an efficient metasurface. By carefully designing the geometry size, a π phase delay is
5 introduced between the long and short axes and the structure then effectively acts as a half wave
6 plate. By using the Jones calculus, a wave plate without coordinate rotation can be expressed as
7
8
9
10
11

$$12 \quad G = \begin{bmatrix} r_l & 0 \\ 0 & r_s e^{i\delta} \end{bmatrix}, \quad (1)$$

13
14 where r_l and r_s are the reflective coefficients along the long and short axes respectively and δ is
15 the phase delay between two mutually orthogonal directions. If circularly polarized (CP) light is
16 incident on the wave plate, the polarization conversion efficiency of the output light with (η_{cross})
17 and without (η_{co}) phase delay (determined by geometric phase) can be expressed as
18
19
20
21
22
23
24
25
26
27

$$28 \quad \begin{cases} \eta_{cross} = \left| \frac{r_l - r_s e^{i\delta}}{2} \right|^2 \\ \eta_{co} = \left| \frac{r_l + r_s e^{i\delta}}{2} \right|^2 \end{cases} \quad (2)$$

29
30 In particular, only if $r_l = r_s = 1$ and $\delta = \pi$, all incident CP light can be converted into the useful
31 cross-polarized part (*i.e.* $\eta_{cross} = 1$ and $\eta_{co} = 0$). Since varying the dimension of the nanobrick
32 affects both the reflectivity along the long and short axes and their phase delay, we need to make
33 a trade-off between high reflectivity and accurate phase delay of π along two orthogonal
34 directions. Figure 1b shows the simulated reflectivity and phase difference of the nanobrick
35 when the normally incident beam is polarized along the long axis and short axis of the nanobrick,
36 respectively. Then we can calculate the efficiency of the reflected co-polarized part and cross-
37 polarized part, as shown in Figure 1c. Significantly, the polarization conversion efficiency can
38 reach as high as 60%, while the unwanted co-polarized light contributing to zero-order
39 diffraction can be suppressed to below 10%. To investigate the high reflection occurring in these
40 metasurfaces, we simulated the distribution of electric and magnetic fields at the cross-section of
41
42
43
44
45
46
47
48
49
50
51
52
53
54
55
56
57
58
59
60

1
2
3 a nanobrick unit cell. As shown in Figure 1d-g, vortex-like electric fields and enhanced magnetic
4 fields inside the nanobrick unit cell indicate the excitation of a magnetic dipole resonance along
5 two axes. Here, the nanobrick is designed with a height H of 220 nm, length L of 290 nm, width
6 W of 140 nm and cellsize C of 400 nm, which leads to a height as low as $\lambda/3$ and a low AR of 1.5
7 along the short axis direction. With the accompanying advantages, *i.e.*, high efficiency, low
8 noise, ultra-compactness and the ease for fabrication, resonant GEMS shows considerable
9 promise for constructing high-performance phase modulators such as holograms.
10
11
12
13
14
15
16
17
18
19
20
21
22
23
24
25
26
27
28
29
30
31
32
33
34
35
36
37
38
39
40
41
42
43
44
45
46
47
48
49
50
51
52
53
54
55
56
57
58
59
60

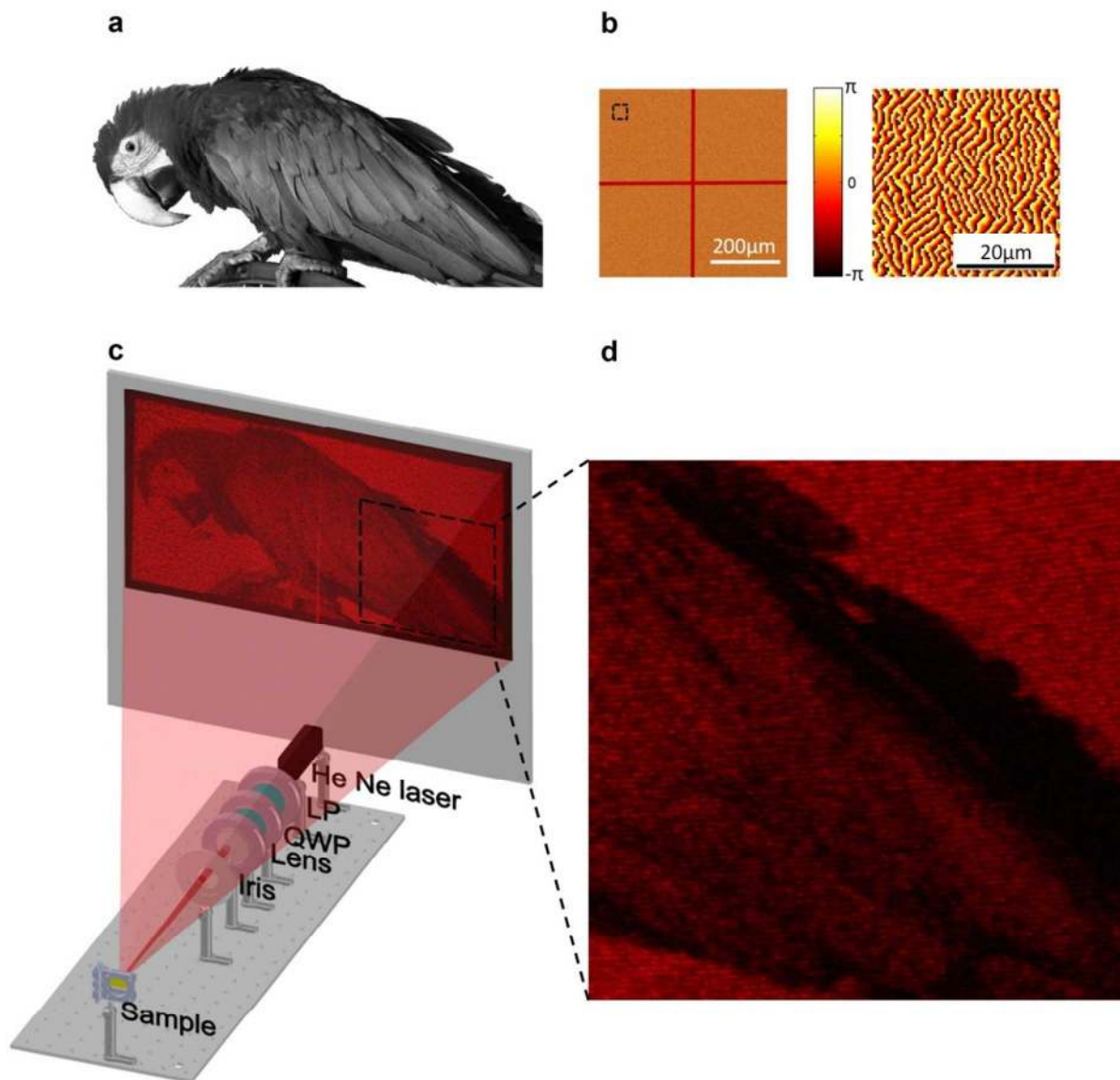
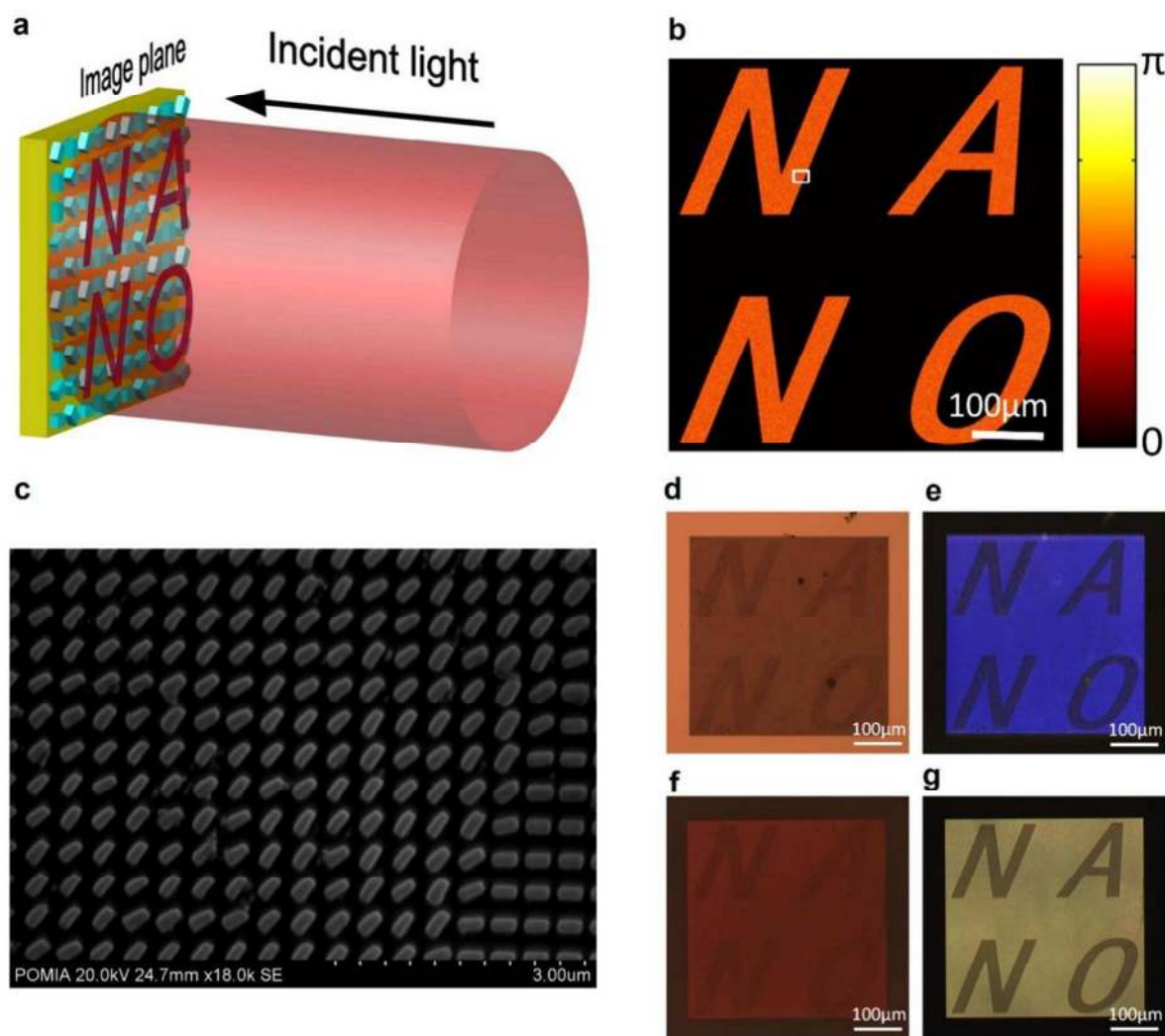


Figure 2. Measurement of Fourier hologram and phase distribution. **a**, The original object of a parrot. **b**, The total and partial zoom-in view (100×100 pixels) of the upper-left corner (in the dashed box) phase distribution designed to generate the target holographic image in the far field. **c**, Illustration of the experimental setup and measured reflection-type Fourier hologram under illumination with circular polarization **d**, The partially zoom-in view of holographic image. The operating wavelength is 632.8 nm and the nanobrick arrays have the same structural parameters as illustrated in Figure 1.

1
2
3 **Results and Discussion.** *Demonstration of Fourier hologram.* A Fourier hologram was designed
4 for CP light at normal incidence, as shown in Figure 2. The reflected beam forms the holographic
5 image (a parrot) at any plane vertical to the optical axis of incident beam in the far field.
6 Moreover, the hologram was designed to create a wide image angle of $40^\circ \times 20^\circ$. To avoid
7 overlap with the zero order spot, the holographic image was designed with an off-axis-angle of
8 10° . The Fourier hologram consists of 2×2 arrays, where the area of each piece is 250×250
9 μm^2 . The phase distribution is designed by the Gerchberg-Saxton algorithm,⁴⁴ as shown in
10 Figure 2b. The experimental (Figure 2c) holographic image, including the zoomed-in view for
11 detail (Figure 2d), shows high fidelity of the metasurface Fourier hologram.
12
13
14
15
16
17
18
19
20
21
22
23
24

25
26 The efficiency measurement experimental setup is shown in Figure S1 in Supporting Information
27 (SI). Theoretically, the meta-hologram has a polarization conversion efficiency of nearly 30% at
28 the measured wavelength of 632.8 nm (as shown in Figure 1c). The measured hologram
29 efficiency, defined as the ratio of the power of refracted holographic image and the power of
30 incident beam, reaches 14%. To further investigate the spectral response of the hologram, we
31 measured the conversion efficiency with a super continuum light source (YSL SC-pro) in the
32 range from 600 to 700 nm in steps of 10 nm. We found that a maximum of 24% can be reached
33 at a wavelength of 660 nm with an efficiency larger than 12% in the measurement range. The
34 peak wavelength agrees well with the simulated one (as shown in Figure 1c), however the
35 efficiency is lower than expected (60%). Such a moderate efficiency may be attributed to several
36 reasons. In general, the fabricated errors may cause inhomogeneous reflectivity of nanobrick
37 arrays and greatly degrade the diffractive performance of the phase-only hologram we designed.
38 Secondly, the diffraction efficiency is hard to be fully optimized that make all the incident beam
39 with phase delay contributing to the reconstruction of holographic image. At last, imperfect
40
41
42
43
44
45
46
47
48
49
50
51
52
53
54
55
56
57
58
59
60

1
2
3 shape (as shown in Figure S2 in SI) and practically larger intrinsic loss of materials will also lead
4 to reduced efficiency. It should be noted that although the conversion efficiency in our sample
5 might be at the lower edge of what is required for practical purposes, it arises from technical
6 issues rather than a theoretical limit in principle. This relatively low value can be improved by
7 more precise fabrication procedures, reducing the extending angles of holographic image and
8 using low-loss dielectric materials (crystalline silicon or TiO_2).
9
10
11
12
13
14
15
16
17
18
19
20
21
22
23
24
25
26
27
28
29
30
31
32
33
34
35
36
37
38
39
40
41
42
43
44
45
46
47
48
49
50
51
52



53 **Figure 3. Working principle, phase distribution and experimental results for GEMS image hologram. a,**
54 **Illustration of working principle of the dielectric GEMS image hologram. b, The designed phase distribution to**
55 **generate a binary word *NANO*. The scale bar is 100 μm . The white box on the border of letter *N* marks the area**
56
57
58
59
60

1
2
3 where SEM image is in the pattern. **c**, SEM image of the fabricated nanobrick arrays. **d, e**, Optical microscope
4 images illuminated by a halogen lamp of microscope and a flashlight of a cellphone, respectively. The height of
5 nanobricks is 220 nm. **f, g**, Optical microscope images illuminated by halogen lamp of the microscope and flashlight
6 of a cellphone, respectively. The height of nanobricks is 150 nm. Other geometry parameters are the same as those
7 used in Figure 1.
8
9
10
11
12
13

14
15 *Demonstration of image hologram with a simple pattern.* Different from Fourier hologram,
16 which produces holographic images in the far field, image holograms can render the target
17 image floating above the sample surface,⁴⁵ which can be observed by the naked eyes (if the
18 sample is big enough) or quite conveniently through an optical microscope. Figure 3a illustrates
19 the working principle of image hologram, where the target image is the word *NANO* as an
20 example. At first, limited by computation resource, a GEMS image hologram was simulated with
21 only 50×50 pixels at a wavelength of 658 nm. The obtained image verifies the performance of
22 our design (as shown in Figure S3 in SI). It is noteworthy that the grayscale difference between
23 the character *NANO* and the background is mainly caused by the phase difference rather than by
24 the magnitude difference due to the equal reflectivity of each nanobrick. Even considering the
25 near-field coupling between neighboring nanobricks, the influences are negligible (as shown in
26 Figure S4 in SI). More importantly, the image hologram we designed is insensitive to the
27 polarization states of incident light. It is known that an incident beam with any polarized states
28 can be a linear combination of two separated sub-beams with orthogonal polarization states, such
29 as left and right circularly polarizations. By using Kirchhoff diffraction formula, we calculated
30 the holographic image *NANO* produced by the phase-only element and we can get almost the
31 same holographic images with left circularly polarized (LCP) and right circularly polarized (RCP)
32
33
34
35
36
37
38
39
40
41
42
43
44
45
46
47
48
49
50
51
52
53
54
55
56
57
58
59
60

1
2
3 incident light (as shown in Figure S5 in SI), which agree well with the theoretical design and
4
5 prove that the polarization-independent characteristics of image hologram.
6
7

8
9 Subsequently, the image hologram was fabricated by standard electron-beam lithography (EBL)
10
11 with a dimension of $500 \times 500 \mu\text{m}^2$ (1250×1250 pixels) and the corresponding phase
12
13 distribution is shown in Figure 3b. The scanning electron microscopy (SEM) image of the
14
15 sample (partial view) is shown in Figure 3c. To investigate the spectral response of the
16
17 metasurface hologram, we used a supercontinuum laser light (YSL SC-pro) to illuminate the
18
19 sample and captured the holographic image by an optical microscope (Nikon LV150N), as
20
21 shown in Figure S6 in SI. We can observe that all of the holographic images are with high
22
23 fidelity and without image distortions or color blurring. The detailed mechanism of these
24
25 important characteristics of image hologram has been investigated in chapter 5 of SI.
26
27
28
29

30
31 To apply to a more natural environment without a restrictive illumination condition (such as
32
33 laser, polarized light, *etc.*), the observation of holographic image under illumination by an
34
35 arbitrary light source was also performed. As shown in Figure 3d, the fabricated hologram was
36
37 first illuminated by a halogen source. It is clear that the word *NANO* can be recognized
38
39 unambiguously. The holographic image was then captured under the illumination of a flash light
40
41 of a cellphone, as shown in Figure 3e. Besides a difference in color hue, the target image shows
42
43 an even better contrast. The differences of the observed images may be attributed to the sample's
44
45 spectral response, diffractive light from broadband source with broad illumination angles and the
46
47 spectral response of charge coupled device (CCD) sensor. Because of the dissimilar spectral
48
49 energy distribution and incident angle of the light sources, their diffraction behavior varies
50
51 significantly.
52
53
54
55
56
57
58
59
60

1
2
3 To further check the robustness to structure height of our design, another GEMS image hologram
4 was fabricated with the same structure parameters and phase distribution but with a reduction in
5 height from 220 to 150 nm, *i.e.* a quarter of operation wavelength. The holographic images were
6 also clearly observed under two types of illumination, as shown in Figures 3f-g. However, a
7 color shift was also observed, which may be caused by the height-induced spectrum variation.
8
9

10
11 It is interesting that the GEMS image hologram is insensitive to the polarization state of incident
12 light, which results from the virtual and real holographic images almost overlapping at the
13 surface of hologram. Therefore, in contrast to Fresnel or Fourier holographic images, image
14 holograms based on GEMS can work under a more relaxed illumination condition, *i.e.*
15 broadband and random polarization states, from incandescent or natural light sources. These
16 advantages make the choice of light source flexible and do not require other optical elements to
17 observe the holographic image (coherent sources such as laser, quarter wave plate, polarizer,
18 *etc.*). With these advantages, the resonant GEMS image hologram technique shows immense
19 prospects in anti-counterfeiting, information security, display and series of fields.
20
21
22
23
24
25
26
27
28
29
30
31
32
33
34
35
36
37
38
39
40
41
42
43
44
45
46
47
48
49
50
51
52
53
54
55
56
57
58
59
60

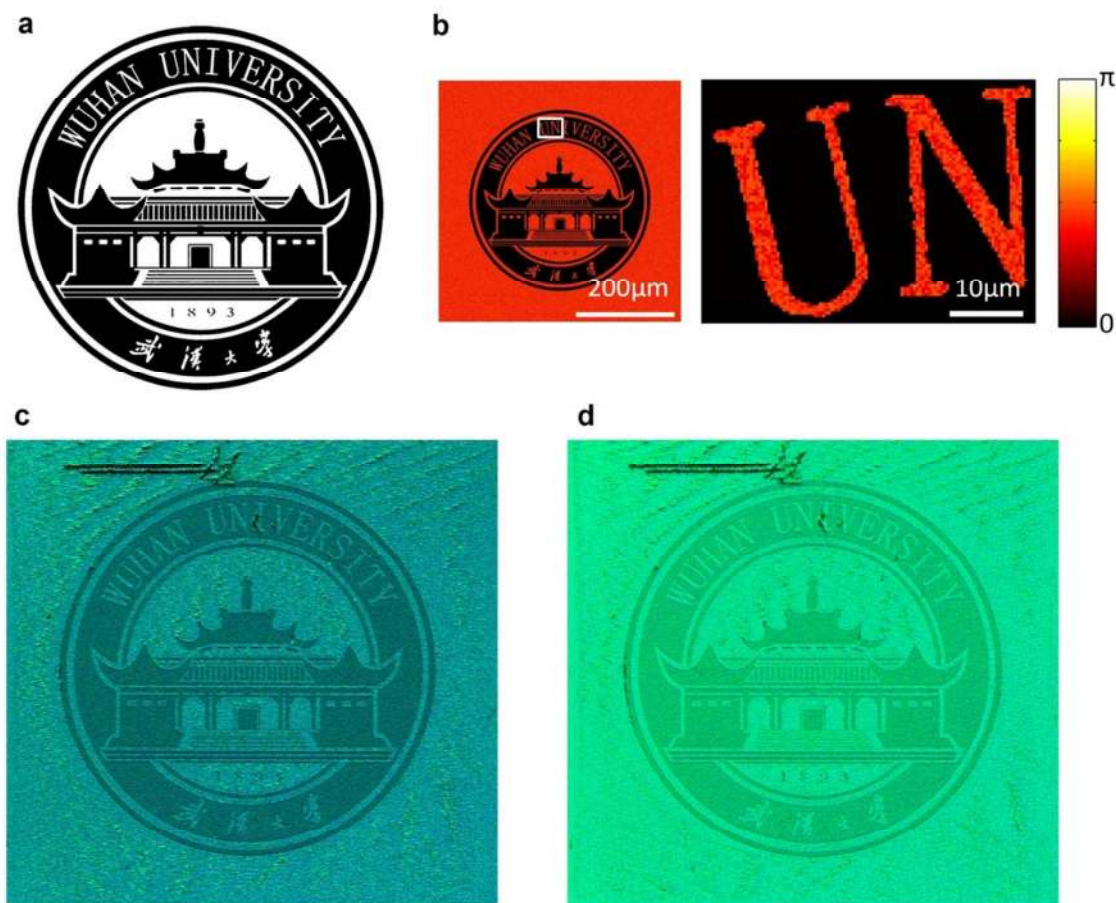


Figure 4. Experimental results for image hologram fabricated on SOI. **a**, The logo of *Wuhan University* was taken as the target image. **b**, The total and partial zoom-in view (in the white box) phase distribution designed to generate the logo. **c**, **d**, Optical microscope images of a resonant GEMS image holograms illuminated by natural light and a flashlight of a cellphone, respectively. The geometry parameters are the same as those used in Figure 1 except that the height is 250 nm here. The logo of *Wuhan University* is used with permission from the Wuhan University.

Demonstration of image hologram with a complicated pattern fabricated on SOI. Silicon on insulator (SOI), being widely used in integrated circuits (IC), is a promising material to make a dielectric GEMS. In our design, a SOI, consisting of a silicon dioxide (SiO_2) layer with a thickness of 2 μm and a silicon cover with a thickness of 250 nm, was employed. The logo of

1
2
3 *Wuhan University* (Figure 4a) was taken as the target image and our designed hologram has
4 dimensions of $500 \times 500 \mu\text{m}^2$ (Figure 4b). The broadband response of GEMS hologram based on
5 SOI is shown in Figure S8 in SI. Since the most promising application of the image hologram
6 fabricated on SOI is anti-counterfeiting, the sample is illuminated by natural light and the
7 captured image is shown in Figure 4c. We also captured the image illuminated by a flashlight of
8 a cellphone, as shown in Figure 4d. Similar to the observations in Figure 3d-g, besides the target
9 image, differences in color also exist when illuminated by different light sources.

10
11
12
13
14
15
16
17
18
19
20
21 **Conclusions.** We have presented a compact reflection-type phase-only meta-hologram using
22 silicon nanostructure-based geometric phase at visible range. The holograms have been verified
23 by Fourier hologram and image hologram with high fidelity. Due to the introduction of dual
24 magnetic dipole resonances, the height of nanobricks in our GEMS can be reduced even down to
25 $\lambda/4$, which significantly relaxes the fabrication burden. Furthermore, the holographic image has
26 also been demonstrated by fabricating the hologram on a commercial SOI substrate, which
27 shows good compatibility with contemporary semiconductor industry technologies.
28 Significantly, due to the wavelength-independent phase response, the designed hologram can be
29 well observed under arbitrary illumination condition such as natural light, which thus may
30 facilitate less stringent applications in the natural setting such as anti-counterfeiting. Finally, we
31 would like to emphasize that such nanobrick-based metasurfaces can be fabricated on a large
32 scale with much lower cost by nano-imprinting, making them promising candidates for large-
33 scale holographic technology.

34
35
36
37
38
39
40
41
42
43
44
45
46
47
48
49
50
51
52
53 **Methods.** *Design of nanobrick unit cell.* The nanobrick unit cell was designed and simulated by
54 CST microwave studio software. In the simulation, a CP plane wave was normally incident onto
55 a single nanobrick with periodic boundary conditions. The reflectivity of the cross-polarized and
56
57
58
59
60

1
2
3
4
5
6
7
8
9
10
11
12
13
14
15
16
17
18
19
20
21
22
23
24
25
26
27
28
29
30
31
32
33
34
35
36
37
38
39
40
41
42
43
44
45
46
47
48
49
50
51
52
53
54
55
56
57
58
59
60

co-polarized parts was collected by field ports. Furthermore, we swept the geometric parameters of the nanobrick (length L , width W , height H and cellsize C) to optimize the performance.

Design of Fourier hologram. In the design, a complex digital image containing a parrot with pixel number of 712×351 and 256 grayscale levels was chosen as holographic target image (Figure 2a). Because of the large angular range, the Rayleigh-Sommerfeld diffraction method was used to simulate the holographic image.^{44, 46} The hologram was pre-compensated to avoid the geometric distortion of pattern. To avoid the formation of laser speckles in the holographic image, the concept of Dammann gratings⁴⁷ was utilized for the hologram design.

Design of image hologram. Balancing the computation complexity against the diffractive performance in our design, the orientation angle α of each nanobrick can be expressed as

$$\begin{cases} \alpha = \frac{\pi}{4} (|B + R|^2 - |B|^2 - |R|^2) \\ R = e^{0.15i\xi} \end{cases}, \quad (3)$$

where B is the brightness of the binary image (B equals 0 or 1), R is the brightness of a reference beam and ξ is a random number satisfies uniform distribution $U[0,1]$. There exist several alternative algorithms to optimize this phase distribution such as simulated annealing method (SA) and genetic algorithm (GA) at the cost of computing time.

Sample fabrication. The samples were fabricated on a silicon-coated SiO_2 substrate with standard EBL. On a $500 \mu\text{m}$ thick fused silica substrate, amorphous silicon was deposited through plasma enhanced chemical vapor deposition (PECVD). The nanobrick structures were patterned in the Copolymer (Microchem, MMA (8.5) MAA EL-8) / PMMA (Microchem, 495 PMMA A2) bilayer positive tone resists by EBL (ELIONIX ELS-7800, 80 kV, 50 pA), and then

1
2
3 Cr (40 nm) was deposited by electron-beam evaporator (KVT KVE-ENS4004), followed by lift-
4
5 off process in hot acetone. Cr was used as etch mask and Cr-free part was removed through dry
6
7 etcher. After the etching process the Cr mask was removed by a Cr etchant. Finally, only silicon
8
9 nanobricks remain on the substrate. In the case of SOI platform (250 nm top silicon and 2 μm
10
11 buried oxide), the procedures are all the same except for silicon deposition process.
12
13

14
15
16 *Experimental setup.* For the Fourier hologram experiment, we used a He-Ne laser with a
17
18 wavelength of 632.8 nm. The CP laser source was incident onto the metasurface hologram, and
19
20 the reflected holographic image was projected onto a white screen 300 mm away from the
21
22 surface of the hologram. We captured the red holographic image using commercial digital
23
24 cameras (PENTAX K50). For the image hologram experiment, we used the optical microscope
25
26 (Nikon LV150N) to observe the holographic image directly without any other optical elements.
27
28
29
30
31
32

33 ASSOCIATED CONTENT

34
35
36
37 [Supporting Information](#). Figures showing the efficiency measurement experiments of Fourier
38
39 hologram, influence of fabrication defects on performance, simulation on the performance of
40
41 image hologram, investigation on the working principle of image hologram and experiment on
42
43 broadband response of the image hologram.
44
45
46

47 AUTHOR INFORMATION

50 **Corresponding Author**

51
52
53 *Email: gxzheng@whu.edu.cn, jsrho@postech.ac.kr, chengwei.qiu@nus.edu.sg
54

55 **Author Contributions**

1
2
3 Z.L., M.Q.M., G.Z., J.R. and C.W.Q. conceived and designed the experiments. Z.L. and G.Z.
4 performed the design and simulation on the metasurfaces. I.K. fabricated the samples. Z.L., Y.W.,
5 G.Z., M.Q.M., M.S.A. and M.S. performed the measurements. Z.L., L.Z., D.L., K.T.N., B.L. and
6 C.W.Q. analyzed the data. Z.L., L.Z., G.Z., S.Z. and C.W.Q. co-wrote the paper. All authors
7 discussed the results and commented on the manuscript. [‡]These authors contributed equally.

16 ACKNOWLEDGMENT

18 L.Z. acknowledges the financial support from Young Talent Recruiting Plans of Xi'an Jiaotong
19 University and the National Natural Science Foundation of China (No. 11604256). I.K.
20 acknowledges the Global Ph.D. fellowship from Korean government (NRF-
21 2016H1A2A1906519). M.Q.M. acknowledges the Information Technology University of the
22 Punjab Lahore, Pakistan for financial support. G.Z. acknowledges the National Natural Science
23 Foundation of China (Nos. 11374235, 11574240, 11774273), the Outstanding Youth Funds of
24 Hubei Province (No. 2016CFA034), the Open Foundation of State Key Laboratory of Optical
25 Communication Technologies and Networks, Wuhan Research Institute of Posts &
26 Telecommunications (No. OCTN-201605), the Fundamental Research Funds for the Central
27 Universities (No. 2042017kf0235). J.R. acknowledges the financial supports from LGD-SNU
28 Incubation program funded by LG Display, Green Science program funded by POSCO, and the
29 National Research Foundation grants (NRF-2015R1C1A1A02036464, NRF-
30 2015R1A5A1037668, CAMM-2014M3A6B3063708) funded by the Ministry of Science, ICT
31 and Future Planning (MSIP) of Korean government. C.Q. would like to acknowledge the support
32 by the National Research Foundation, Prime Minister's Office, Singapore under its Competitive
33 Research Program (CRP Award No. NRF-CRP15-2015-03). We also like to thank Ali Akbar for
34 his suggestions on optical instruments.

1
2
3 REFERENCES4
5 REFERENCES

- 6
7
8 1. Chong, K. E.; Staude, I.; James, A.; Dominguez, J.; Liu, S.; Campione, S.; Subramania, G. S.;
9
10 Luk, T. S.; Decker, M.; Neshev, D. N.; Brener, I.; Kivshar, Y. S. Polarization-Independent
11
12 Silicon Metadevices for Efficient Optical Wavefront Control. *Nano Lett.* **2015**, *15*, 5369-5374.
13
14
15 2. Li, Q.; Dong, F.; Wang, B.; Gan, F.; Chen, J.; Song, Z.; Xu, L.; Chu, W.; Xiao, Y.; Gong, Q.;
16
17 Li, Y. Polarization-Independent and High-Efficiency Dielectric Metasurfaces for Visible Light.
18
19 *Opt. Express* **2016**, *24*, 16309-16319.
20
21
22 3. Yu, N.; Genevet, P.; Kats, M. A.; Aieta, F.; Tetienne, J.; Capasso, F.; Gaburro, Z. Light
23
24 Propagation with Phase Discontinuities: Generalized Laws of Reflection and Refraction. *Science*
25
26 **2011**, *334*, 333-337.
27
28
29 4. Aieta, F.; Genevet, P.; Kats, M. A.; Yu, N.; Blanchard, R.; Gaburro, Z.; Capasso, F.
30
31 Aberration-free Ultrathin Flat Lenses and Axicons at Telecom Wavelengths Based on Plasmonic
32
33 Metasurfaces. *Nano Lett.* **2012**, *12*, 4932-4936.
34
35
36 5. Pors, A.; Nielsen, M. G.; Eriksen, R. L.; Bozhevolnyi, S. I. Broadband Focusing Flat Mirrors
37
38 Based on Plasmonic Gradient Metasurfaces. *Nano Lett.* **2013**, *13*, 829-834.
39
40
41 6. Yang, Y.; Wang, W.; Moitra, P.; Kravchenko, I. I.; Briggs, D. P.; Valentine, J. Dielectric
42
43 Meta-Reflectarray for Broadband Linear Polarization Conversion and Optical Vortex
44
45 Generation. *Nano Lett.* **2014**, *14*, 1394-1399.
46
47
48 7. Arbabi, A.; Horie, Y.; Bagheri, M.; Faraon, A. Dielectric Metasurfaces for Complete Control
49
50 of Phase and Polarization with Subwavelength Spatial Resolution and High Transmission. *Nat.*
51
52 *Nanotechnol* **2015**, *10*, 190-937.
53
54
55
56
57
58
59
60

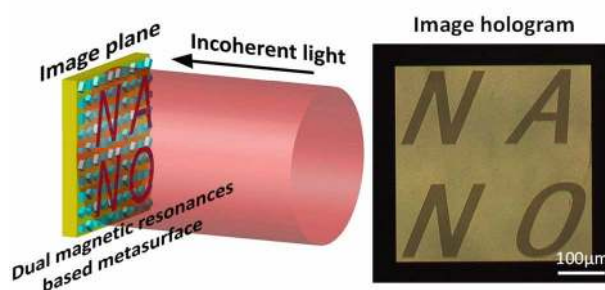
- 1
2
3 8. Wang, Q.; Zhang, X.; Xu, Y.; Gu, J.; Li, Y.; Tian, Z.; Singh, R.; Zhang, S.; Han, J.; Zhang,
4 W. Broadband Metasurface Holograms: Toward Complete Phase and Amplitude Engineering.
5
6 *Sci. Rep.* **2016**, *6*, 32867.
7
- 8
9
10 9. Khorasaninejad, M.; Zhuit, A. Y.; Roques-Carmes, C.; Chen, W. T.; Oh, J.; Mishra, I.;
11
12 Devlin, R. C.; Capasso, F. Polarization-Insensitive Metalenses at Visible Wavelengths. *Nano*
13
14 *Lett.* **2016**, *16*, 7229-7234.
15
- 16
17 10. Yu, N.; Capasso, F. Flat Optics with Designer Metasurfaces. *Nat. Mater.* **2014**, *13*, 139-150.
18
- 19
20 11. Zheng, G.; Liu, G.; Kenney, M. G.; Li, Z.; He, P.; Li, S.; Ren, Z.; Deng, Q. Ultracompact
21
22 High-Efficiency Polarising Beam Splitter Based on Silicon Nanobrick Arrays. *Opt. Express*
23
24 **2016**, *24*, 6749-6757.
25
- 26
27 12. Zhou, Z.; Li, J.; Su, R.; Yao, B.; Fang, H.; Li, K.; Zhou, L.; Liu, J.; Stellinga, D.; Reardon, C.
28
29 P.; Krauss, T. F.; Wang, X. Efficient Silicon Metasurfaces for Visible Light. *ACS Photonics*
30
31 **2017**, *4*, 544-551.
32
- 33
34 13. Wu, C.; Arju, N.; Kelp, G.; Fan, J. A.; Dominguez, J.; Gonzales, E.; Tutuc, E.; Brener, I.;
35
36 Shvets, G. Spectrally Selective Chiral Silicon Metasurfaces Based on Infrared Fano Resonances.
37
38 *Nat. Commun.* **2014**, *5*, 3892.
39
- 40
41 14. West, P. R.; Stewart, J. L.; Kildishev, A. V.; Shalaev, V. M.; Shkunov, V. V.; Strohkendl, F.;
42
43 Zakharenkov, Y. A.; Dodds, R. K.; Byren, R. All-Dielectric Subwavelength Metasurface
44
45 Focusing Lens. *Opt. Express* **2014**, *22*, 26212-26221.
46
- 47
48 15. Deng, Z.; Zhang, S.; Wang, G. P. A Facile Grating Approach Towards Broadband, Wide-
49
50 Angle and High-Efficiency Holographic Metasurfaces. *Nanoscale* **2016**, *8*, 1588-1594.
51
52
53
54
55
56
57
58
59
60

16. Mehmood, M. Q.; Mei, S.; Hussain, S.; Huang, K.; Siew, S. Y.; Zhang, L.; Zhang, T.; Ling, X.; Liu, H.; Teng, J.; Danner, A.; Zhang, S.; Qiu, C. Visible-Frequency Metasurface for Structuring and Spatially Multiplexing Optical Vortices. *Adv. Mater.* **2016**, *28*, 2533-2539.
17. Mei, S.; Mehmood, M. Q.; Hussain, S.; Huang, K.; Ling, X.; Siew, S. Y.; Liu, H.; Teng, J.; Danner, A.; Qiu, C. Flat Helical Nanosieves. *Adv. Funct. Mater.* **2016**, *26*, 5255-5262.
18. Chen, X.; Huang, L.; Muehlenbernd, H.; Li, G.; Bai, B.; Tan, Q.; Jin, G.; Qiu, C.; Zhang, S.; Zentgraf, T. Dual-Polarity Plasmonic Metalens for Visible Light. *Nat. Commun.* **2012**, *3*, 1198.
19. Wang, Y.; Pu, M.; Zhang, Z.; Li, X.; Ma, X.; Zhao, Z.; Luo, X. Quasi-Continuous Metasurface for Ultra-Broadband and Polarization-Controlled Electromagnetic Beam Deflection. *Sci. Rep.* **2015**, *5*, 17733.
20. Lin, D.; Fan, P.; Hasman, E.; Brongersma, M. L. Dielectric Gradient Metasurface Optical Elements. *Science* **2014**, *345*, 298-302.
21. Khorasaninejad, M.; Crozier, K. B. Silicon Nanofin Grating as a Miniature Chirality-Distinguishing Beam-Splitter. *Nat. Commun.* **2014**, *5*, 5386.
22. Li, Z.; Zheng, G.; He, P.; Li, S.; Deng, Q.; Zhao, J.; Ai, Y. All-Silicon Nanorod-Based Dammann Gratings. *Opt. Lett.* **2015**, *40*, 4285-4288.
23. Khorasaninejad, M.; Chen, W. T.; Oh, J.; Capasso, F. Super-Dispersive Off-Axis Metalenses for Compact High Resolution Spectroscopy. *Nano Lett.* **2016**, *16*, 3732-3737.
24. Khorasaninejad, M.; Chen, W. T.; Devlin, R. C.; Oh, J.; Zhu, A. Y.; Capasso, F. Metalenses at Visible Wavelengths: Diffraction-Limited Focusing and Subwavelength Resolution Imaging. *Science* **2016**, *352*, 1190-1194.

- 1
2
3
4
5
6
7
8
9
10
11
12
13
14
15
16
17
18
19
20
21
22
23
24
25
26
27
28
29
30
31
32
33
34
35
36
37
38
39
40
41
42
43
44
45
46
47
48
49
50
51
52
53
54
55
56
57
58
59
60
25. Huang, K.; Dong, Z.; Mei, S.; Zhang, L.; Liu, Y.; Liu, H.; Zhu, H.; Teng, J.; Luk'Yanchuk, B.; Yang, J. K. W.; Qiu, C. Silicon Multi-Meta-Holograms for the Broadband Visible Light. *Laser Photonics Rev.* **2016**, *10*, 500-509.
26. Ke, Y.; Liu, Y.; He, Y.; Zhou, J.; Luo, H.; Wen, S. Realization of Spin-Dependent Splitting with Arbitrary Intensity Patterns Based on All-Dielectric Metasurfaces. *Appl. Phys. Lett.* **2015**, *107*, 0411074.
27. Ye, W.; Zeuner, F.; Li, X.; Reineke, B.; He, S.; Qiu, C.; Liu, J.; Wang, Y.; Zhang, S.; Zentgraf, T. Spin and Wavelength Multiplexed Nonlinear Metasurface Holography. *Nat. Commun.* **2016**, *7*, 11930.
28. Li, X.; Chen, L.; Li, Y.; Zhang, X.; Pu, M.; Zhao, Z.; Ma, X.; Wang, Y.; Hong, M.; Luo, X. Multicolor 3D Meta-Holography by Broadband Plasmonic Modulation. *Sci. Adv.* **2016**, *2*, e1601102.
29. Wan, W.; Gao, J.; Yang, X. Full-Color Plasmonic Metasurface Holograms. *ACS Nano* **2016**, *10*, 10671-10680.
30. Zhao, W.; Liu, B.; Jiang, H.; Song, J.; Pei, Y.; Jiang, Y. Full-Color Hologram Using Spatial Multiplexing of Dielectric Metasurface. *Opt. Lett.* **2016**, *41*, 147-150.
31. Zheng, G.; Muehlenbernd, H.; Kenney, M.; Li, G.; Zentgraf, T.; Zhang, S. Metasurface Holograms Reaching 80% Efficiency. *Nat. Nanotechnol.* **2015**, *10*, 308-312.
32. Wen, D.; Yue, F.; Li, G.; Zheng, G.; Chan, K.; Chen, S.; Chen, M.; Li, K. F.; Wong, P. W. H.; Cheah, K. W.; Pun, E. Y. B.; Zhang, S.; Chen, X. Helicity Multiplexed Broadband Metasurface Holograms. *Nat. Commun.* **2015**, *6*, 8241.
33. Ni, X.; Kildishev, A. V.; Shalaev, V. M. Metasurface Holograms for Visible Light. *Nat. Commun.* **2013**, *4*, 2807.

- 1
2
3 34. Huang, L.; Chen, X.; Mühlenbernd, H.; Zhang, H.; Chen, S.; Bai, B.; Tan, Q.; Jin, G.;
4
5 Cheah, K.; Qiu, C.; Li, J.; Zentgraf, T.; Zhang, S. Three-Dimensional Optical Holography Using
6
7 a Plasmonic Metasurface. *Nat. Commun.* **2013**, *4*, 2808.
8
9
10 35. Ginn, J. C.; Brener, I.; Peters, D. W.; Wendt, J. R.; Stevens, J. O.; Hines, P. F.; Basilio, L. I.;
11
12 Warne, L. K.; Ihlefeld, J. F.; Clem, P. G.; Sinclair, M. B. Realizing Optical Magnetism from
13
14 Dielectric Metamaterials. *Phys. Rev. Lett.* **2012**, *108*, 0974029.
15
16
17 36. Liu, S.; Sinclair, M. B.; Mahony, T. S.; Jun, Y. C.; Campione, S.; Ginn, J.; Bender, D. A.;
18
19 Wendt, J. R.; Ihlefeld, J. F.; Clem, P. G.; Wright, J. B.; Brener, I. Optical Magnetic Mirrors
20
21 without Metals. *Optica* **2014**, *1*, 250-256.
22
23
24 37. Zhao, Q.; Zhou, J.; Zhang, F.; Lippens, D. Mie Resonance-Based Dielectric Metamaterials.
25
26 *Mater. Today* **2009**, *12*, 60-69.
27
28
29 38. Moitra, P.; Slovick, B. A.; Li, W.; Kraychencko, I. I.; Briggs, D. P.; Krishnamurthy, S.;
30
31 Valentine, J. Large-Scale All-Dielectric Metamaterial Perfect Reflectors. *ACS Photonics* **2015**,
32
33 *2*, 692-698.
34
35
36 39. Shalaev, M. I.; Sun, J.; Tsukernik, A.; Pandey, A.; Nikolskiy, K.; Litchinitser, N. M. High-
37
38 Efficiency All-Dielectric Metasurfaces for Ultra-Compact Beam Manipulation in Transmission
39
40 Mode. *Nano Lett.* **2015**, *15*, 6261-6266.
41
42
43 40. Kuznetsov, A. I.; Miroshnichenko, A. E.; Fu, Y. H.; Zhang, J.; Luk Yanchuk, B. Magnetic
44
45 Light. *Sci. Rep.* **2012**, *2*, 492.
46
47
48 41. Kuznetsov, A. I.; Miroshnichenko, A. E.; Brongersma, M. L.; Kivshar, Y. S.; Luk Yanchuk,
49
50 B. Optically Resonant Dielectric Nanostructures. *Science* **2016**, *354*, 2472.
51
52
53
54
55
56
57
58
59
60

- 1
2
3
4
5
6
7
8
9
10
11
12
13
14
15
16
17
18
19
20
21
22
23
24
25
26
27
28
29
30
31
32
33
34
35
36
37
38
39
40
41
42
43
44
45
46
47
48
49
50
51
52
53
54
55
56
57
58
59
60
42. Yu, Y. F.; Zhu, A. Y.; Paniagua-Dom, R.; Fu, Y. H.; Luk Yanchuk, B.; Kuznetsov, A. I. High-Transmission Dielectric Metasurface with 2π Phase Control at Visible Wavelengths. *Laser Photonics Rev.* **2015**, *9*, 412-418.
43. Decker, M.; Staude, I.; Falkner, M.; Dominguez J.; Neshev, D. N.; Brener, I.; Pertsch, T.; Kivshar, Y. S. High-Efficiency Dielectric Huygens' Surfaces. *Adv. Opt. Mater.* **2015**, *3*, 813-820.
44. Gerchberg, R. W.; Saxton, W. O. A Practical Algorithm for the Determination of Phase from Image and Diffraction Plane Pictures. *Optik* **1972**, *35*, 237.
45. Rebane, A.; Drobizhev, M.; Sigel, C. Single Femtosecond Exposure Recording of an Image Hologram by Spectral Hole Burning in an Unstable Tautomer of a Phthalocyanine Derivative. *Opt. Lett.* **2000**, *25*, 1633-1635.
46. Shen, F.; Wang, A. Fast-Fourier-Transform Based Numerical Integration Method for the Rayleigh–Sommerfeld Diffraction Formula. *Appl. Opt.* **2006**, *45*, 1102-1110.
47. Dammann, H.; Görtler, K. High-Efficiency In-Line Multiple Imaging by Means of Multiple Phase Holograms. *Opt. Commun.* **1971**, *3*, 312–315.



For Table of Contents Only